Novel Robotic Platform for Affordable and Customizable Testing and Prototyping

Nagpal, Jayesh
Department of Mechanical and Automation Engineering, Maharaja Agrasen Institute of Technology

Lal, Roop
Department of Mechanical Engineering, Delhi Technological University

Rana, Ramakant
Department of Mechanical and Automation Engineering, Maharaja Agrasen Institute of Technology

https://doi.org/10.5109/6782148

出版情報：Evergreen. 10 (1), pp.454-462, 2023-03. 九州大学グリーンテクノロジー研究教育センター
バージョン：

Novel Robotic Platform for Affordable and Customizable Testing and Prototyping

Jayesh Nagpal[1], Roop Lal[2], Ramakant Rana[1, *]

[1]Department of Mechanical and Automation Engineering, Maharaja Agrasen Institute of Technology, Delhi-110086, India

[2]Department of Mechanical Engineering, Delhi Technological University, Delhi-110042, India

*Author to whom correspondence should be addressed:
E-mail: 7ramakant@gmail.com

(Received July 12, 2022; Revised January 24, 2023; accepted January 24, 2023).

Abstract: The robotic platforms currently available for testing the software stability and functionality are expensive and are not highly customizable in terms of hardware. This makes the platforms out of reach of the grasp of researchers and small-scale start-ups. We have proposed a design of a robotic platform that is easier to manufacture and cheaper to build (totaling under USD 1000). The components used are easily available and are cheaper as compared to the components of currently available robotic solutions. The design features of the platform are explored along with factors and features that make the proposed platform favorable to small-scale researchers and start-ups. The components of the platform are discussed along with their purpose in the design. A model that is highly customizable, easy and cheap to manufacture, and capable of carrying out general tasks of navigation and manipulation was made. Scaling the model physically down to making its smallest gearbox (in wrist actuator) of about 10 cm in diameter, was also made possible using the design principles proposed in the paper. Further scope of improvement and ideas for the next version design were also explored.

Keywords: Robotics, Design, Robotic Arm, Degree of Freedom.

1. Introduction

In robotics research, the main constituents have always been the code that runs the robot and the body that the code moves. These two aspects of robotics have been interdependent for a while now, but this has been changing over the last few years with the development of simulation and visualization software[1,2]. This software has allowed the software developers to run a program that is meant to be deployed to real hardware, on a simulated model of the target robot and its environment[3,4]. Though in a simulation, every parameter is set to replicate the performance of the robot in the real world, there are always some caveats [5,6].

The development of a testing platform that is capable of performing general applications and which is simple enough to be customized to the specific application for prototyping or testing purposes is the goal of our research [7,8]. There hasn't been a robot model which is highly customizable in terms of hardware. In this paper, we are proposing a design of a robotic platform that is capable of general manipulation and navigation tasks, along with options for customization and design changes for specific experimentations or applications [9, 10]. The proposed model is highly customizable in the sense that the user can control or change the physical size of the model according to the needs, which has not been seen in many available robotic models. The compatibility of the design with different hardware components, like actuators or motors and sensors, is also not commonly seen in such platforms. The cost of manufacturing the model was targeted to be kept under USD 1000.

2. Problem Statement

As discussed, the simulations have been a solution for testing the software on virtual hardware before investing in hardware development further than prototyping, but the simulation has its flaws [11,12].

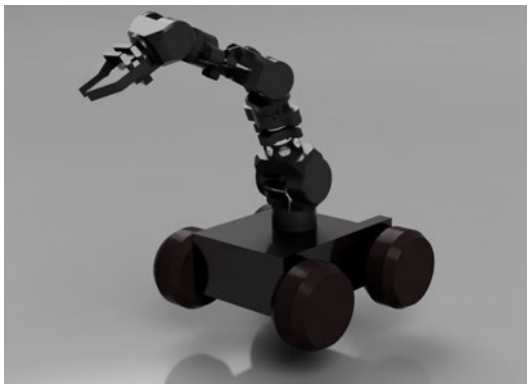

Fig. 1: Render of the Proposed Robotic Platform

The simulation that is developed to simulate the "life-like" environment for the experiments requires computations that can only be performed by expensive high-end hardware[13]. This elevates the overall cost of only testing the program before deployment. This might not be an issue for an enterprise but for a start-up or an individual with a self-funded project, this might be the limiting factor that has held them back from deploying their solution. Moreover, there are always some changes and tuning that are required to be done in the program while porting the software from simulation to real-world hardware [14].

The solution is to develop a robotic platform that can be used to test the software before deployment, but the platform needs to be cheap, easy to acquire, flexible, and easily customizable for specific applications[15]. Such a platform can present itself as a test bench for developers at a small scale and help tweak and prepare their software for deployment [16].

3. Hardware Description

The target function of the platform is to perform the tasks of general manipulation and navigation [17]. For this the platform design is based on a robotic arm with 6 degrees of freedom, mounted on a moving base [18]. This platform is targeted to be manufactured using 3D printing, which allows us to make parts lighter and cheaper [19]. Another benefit of using 3D printing is that we have rapid prototyping at our disposal and hence, customization for specific applications can be done very easily and rapidly[20]. The hardware has been divided into two segments - mechanical and electronic hardware[21].

3.1 Electronics

The electronics for any robotic platform can be the driving factor for alleviation of the overall cost of the hardware [18]. The electronics are half of what determines the performance of a robotic platform [20]. Components like motors, motor drivers, encoders, etc. determine the accuracy of the motion of a robot's joints and also the torque or power that the individual joint can transmit [21].

Table 1. Electronic Components Used in the Platform.

Electronic Component	Model of Component
DC Motor (Shoulder and Elbow Joints)	RS775 DC Motor 12V
DC Motor (Wrist Joint)	RS540 DC Motor 12V
Gripper Motor	MG995 Servo Motor
Encoder Sensor	49E Hall Sensor
Homing Sensor	49E Hall Sensor
Motor Driver	BTS7960 Motor Driver
Microcontroller	Arduino Mega2560
Main Board	NVidia Jetson Nano

The components chosen for our platform were defined by the guideline to keep the overall manufacturing cost of the build as low as possible while keeping the platform functional enough to perform the targeted tasks. Table 1 presents the list of components that we have chosen for build [22].

For the naming convention for the joints, we are bridging the comparison between our robotic arm and the human arm, where the gripper corresponds to a human hand and the base joint of the robotic arm corresponds to the shoulder joint. The wrist joint has been decided to be powered by a RS 540 DC motor. The motor was chosen for its cheaper cost along with its high RPM and lightweight. The weight (0.15 Kg) allowed us to use this motor for the wrist joint of our robotic arm.

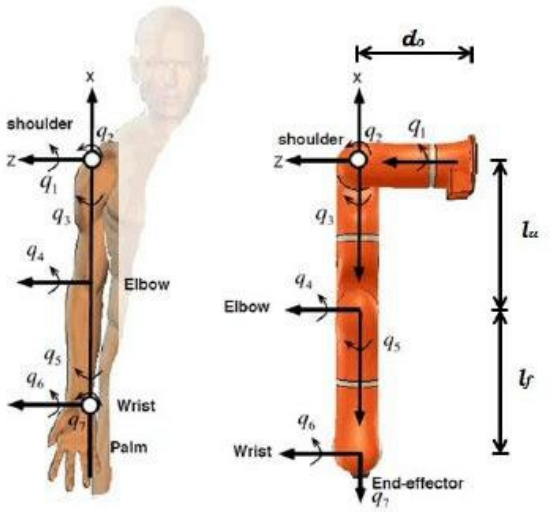

Fig 2. Comparison of a Robotic Arm to a Human Arm for the Naming Convention of Joints.

The motor for the shoulder and the elbow joints was chosen to be a RS 775 DC motor. This motor was chosen

for its low current consumption and high torque output. The high availability of motors also benefits the ease of manufacturing the platform. This motor is also used as the main driver for the base of the platform [23].

To drive the said motors, the motor driver chosen was BTS7960 Motor Driver. This double half-h-bridge motor driver allows the control of the motor using PWM signals from a microcontroller. The said driver was chosen for its high current and voltage limits [24]. The motors chosen are capable of drawing about 6 amperes of current at full load at 12 volts; most of the widely available drivers such as L298 drivers are only capable of handling 3 amperes of current at most. Also, the high voltage limit of the BTS7960 Motor Driver allows for easy upgrade to 24 Volt DC motors or higher voltage DC motors if required [25].

The encoders chosen for position tracking of the motors and joints are the 49E Analog Hall Sensors. The sensors were chosen to keep the cost of the encoder low. The encoder setup of our actuators depends on 6 equally spaced magnets mounted on the planet gear of the gearbox. This allows the sensor to be near the magnets and detect changes in the magnetic field due to the rotation of the planet gear. This setup allows the microcontroller to keep track of the rotational position of the joint with granular precision. The precision of this setup is no way near to what one can get through the use of stepper motors, but the cost of the setup is a lot cheaper as compared to the one required to drive stepper motors [26, 27].

The microcontroller - Arduino Mega, was chosen for the availability of PWM and Analog pins required to drive the motor controllers and to take input from the hall sensors respectively. Also, the ease of programming the microcontroller and the well-established community for support helped in making this choice [28]. The main board of the robot is an NVidia Jetson Nano. This board is the center for all the processing and computing of the robotic platform. As the objective of the platform is to be used for research and development of manipulation and navigation applications, this board will be suitable for running a Robot Operating System (ROS) which is widely used software in research and development in the robotic industry. The board will also provide great expandability and flexibility in terms of sensors and communication in the case of a multi-robot network.

3.2 Mechanical Description

The robotic arm and the mobile base of the robotic platform have been designed by us from scratch. The robotic arm has 6 degrees of freedom which when combined with the planar motion that the mobile base provides, is capable of performing manipulation tasks while not being bound by a permanently mounted position. The design has been developed while keeping the ease of assembly, cheap manufacturing, and easy maintenance of the components of the platform. The platform is designed to be scalable in either direction. The mechanical components' scale depends on the electronic components that the user might decide to power the platform with. For structural rigidity, 8mm chrome-plated rods are used across the structure of joint actuators. Such rods have been used in 3D Printers for sturdy hotend axes. The mechanical design of the platform has major components - the robotic arm and the mobile platform.

3.2.1 Mobile Base

The mobile base has dimensions - 400x300x150 mm (lxbxh). The base has 4 wheels of diameter 160mm that supports the whole weight of the robot. The base is driven by four RS 775 DC motors, which engage the axles of wheels via a belt-pulley reduction assembly.

The base is responsible for housing all the electronics except the motors and sensors of the robot. The power delivery of the robot is handled by two DC 120W power supplies. These are housed in the front portion of the base. The base also has a maintenance hatch to easily access all the electronics housed in the base. This will allow easy maintenance of the electronics. For cooling all the electronics stored in the base, four 120mm computer fans are attached in the exhaust configuration at the bottom panel of the base; this setup will provide sufficient cooling for all the electronics.

The base maintenance hatch also has all the female connectors used to connect all the electronics in the robotic arm to the control panel in the base. The connectors are 10-pin ATX connectors. These are used for systematic cable management and also for easy disassembling or replacement of any components of the robotic platform.

3.2.1 Robotic Arm

The robotic arm as mentioned above has 6 degrees of freedom which are demonstrated in Fig 3. The joints of the robotic arm are linearly arranged concerning each other, i.e. when the arm is stretched to full extension, all the joints are placed along a single axis. This arrangement allows the arm to be highly balanced along the axis and also the inverse kinematic solutions are easier to compute for such an arrangement. The publications presented great insight into the dynamics and analysis of the design of the robotic arm. The robotic arm has a wrist, an elbow, a shoulder, and a gripper.

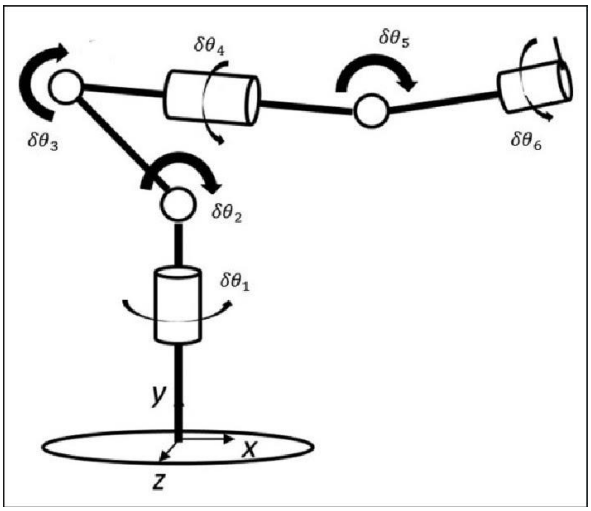

Fig 3. 6 Degrees of Freedom in a Robotic Arm

3.3.2.1 Joint Actuator

All three joint actuators are identical in design but are just scaled according to the gearbox dimensions. The identical design of the actuators proves the scalability of the actuator design. The joint actuator consists of two degrees of freedom each. The setups for each of the degrees are similar in design to each other along with the constituents of the components required to assemble them. This allows ease in manufacturing the actuator without much change in the manufacturing setup. Each actuator consists of a pair of mechanical or structural components mentioned in Table 2.

Table 2. Mechanical and Structural Components in a Joint Actuator.

Component Name	**Naming Convention for *Theta* and *Fi*. Components**
Output Ring Cover (ORC)	*Theta*-ORC Link; *Fi*-ORC
Input Ring Cover (IRC)	*Theta*-IRC; *Fi*-IRC
Motor Support	*Theta*-Motor Support; *Fi*-Motor Support
Gearbox	*Same for both*
6201-2RS Ball Bearing	*Same for both*

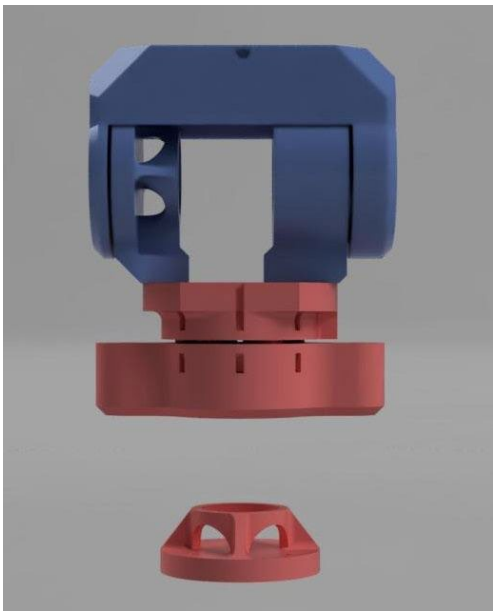

Fig 4. Blue - *Theta* Portion; Red - *Fi* Portion. The motors and rods have been removed from the render. (top, blue) *Theta*-ORC Link

The naming convention for the actuator components uses a prefix for distinguishing between the two degrees of freedom to avoid confusion while referring to the components. The prefixes are - *theta* and *fi*. The components for demonstration purposes are shown in Fig 4 with color coding for distinguishing between *theta* and *fi* components. The axis about which the *theta*-gearbox revolves is named the *theta-axis* and the one about which the *fi*-gearbox revolves is named the *fi-axis*.

The components are designed to be 3D printed without the use of support material for any of the parts. All the components of the robotic platform that are required to be 3D Printed can be printed without the need for support material. This has been accomplished by the use of sacrificial bridging and other techniques to make the parts printable without support material (Fig 5.) This feature of design allows for much faster printing of parts and reduces the wastage of material while printing. This also reduces the post-processing of 3D Printed parts.

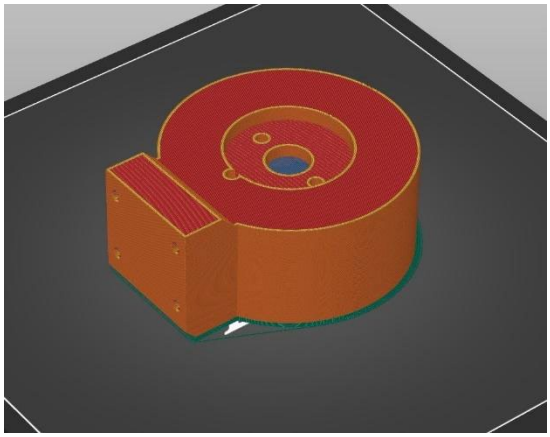

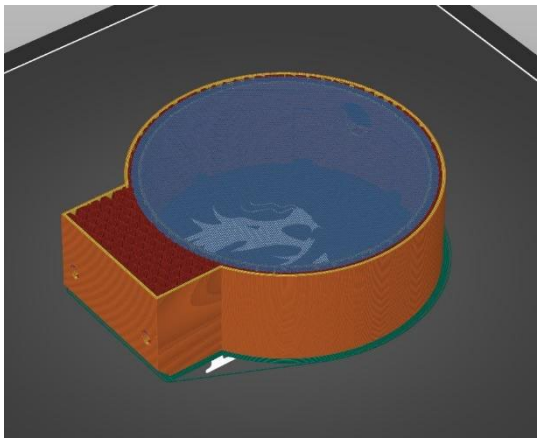

Fig 5. Top - the orientation of *Theta*-IRC for printing without support material. Bottom - The sacrificial bridging (blue) for making the holes in the model printable without support material.

- Gearbox

The gearbox chosen for the platform is a split-ring compound planetary gearbox. Though the proposed platform can be built using any type of gearbox due to the flexibility of the design, we went with a split-ring compound planetary gearbox due to the benefits it provides us with as compared to the other types of gearboxes used in robotics applications. Other gearboxes considered for the application were - harmonic drive gearbox, cycloidal gearbox, and compound cycloidal gearbox. Many factors presented were considered for making the choice of selecting the gearbox which would have been well suited for our proposed platform.

The harmonic drive gearbox has been praised for its high-density reduction with zero backlashes for years now. Its applications range from being used in space rovers or satellites to precise robotic manipulators. The main drawback of the harmonic drive that led us to reject this design was the lack of a proper method or design procedure to make this gearbox 3D Printable. Many attempts had been made to make the flexible spline using TPU or Flexible Filament for 3D Printing but the teeth skipping and low torque transmission were unacceptable drawbacks of the design.

The cycloidal drive, though not providing as dense reduction as the harmonic drives, design of the cycloidal gearbox is simple enough to be 3D Printed with precision. But the drawbacks the said gearbox introduced were again not in favor of being used in our design. The inherited drawback of the cycloidal drive is the wear of the cycloidal disks in the gearbox. The constant rubbing of plates and their teeth rolling against the outer ring of the gearbox lead to a high wear rate of cycloidal plates, and this flaw is elevated in the 3D Printed version of the cycloidal gearbox. Moreover, to reduce the friction of the plates, the use of bearings in the outer ring of the gearbox introduces weight to the whole assembly which makes the movement of the actuator by the other joints very difficult. Because of these reasons, the cycloidal and compound cycloidal drive gearboxes were rejected. The split-ring compound planetary gearbox was our chosen gearbox because it was the only gearbox that could be easily 3D Printed and has a high reduction density that is required by our design. The gearbox consists of two stages of the planetary gear arrangement. The stages have different gear modules and the number of teeth as compared to each other and hence result in differential gear reduction. The gearbox configuration for each joint actuator is given in Table 3.

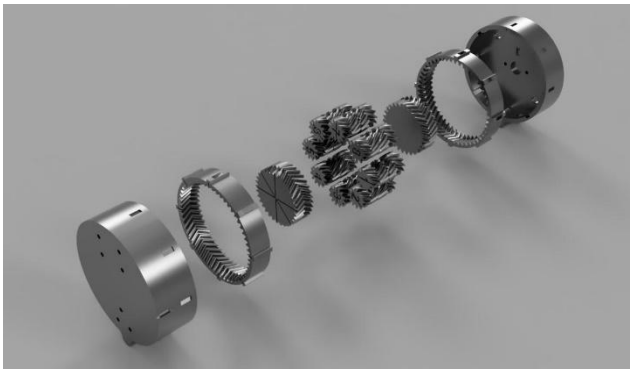

Fig 6. (from left) Output Ring Cover (ORC), Output Ring Gear, Output Sun Gear, Planet Gears (1-8), Input Sun Gear, Input Ring Gear, and Input Ring Cover (IRC)

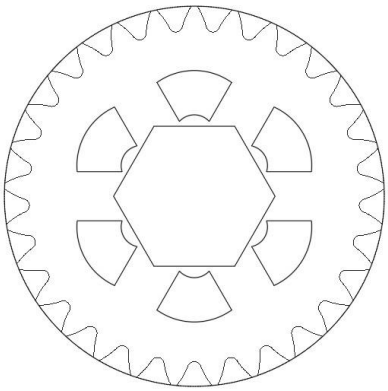

Fig 7. Input Sun Gear Drawing, the slots around the central Hexagon are for magnets for the encoder setup.

Table 3 a. The Gearbox Configuration for Each Actuator Joint (Wrist Actuator Joint Gearbox Configuration)

Helix Angle - 30 degrees	Gear Ratio - 53.39	Number of Planets - 4
	Input Stage	Output Stage
Gear Module	1.6	1.223
Sun Gear Teeth Count	16	22
Ring Gear Teeth Count	36	46

Planet Gear Teeth Count	10	12

Table 3 b. The Gearbox Configuration for Each Actuator Joint (Elbow Actuator Joint Gearbox Configuration)

Helix Angle - 30 degrees	Gear Ratio - 238.235	Number of Planets - 6
	Input Stage	Output Stage
Gear Module	1.8	1.4727
Sun Gear Teeth Count	17	21
Ring Gear Teeth Count	37	45
Planet Gear Teeth Count	10	12

Table 3 c. The Gearbox Configuration for Each Actuator Joint (Shoulder Actuator Joint Gearbox Configuration)

Helix Angle - 30 degrees	Gear Ratio - 424.827	Number of Planets - 8
-	Input Stage	Output Stage
Gear Module	1.8	1.6363
Sun Gear Teeth Count	29	32
Ring Gear Teeth Count	51	56
Planet Gear Teeth Count	11	12

The procedure of designing the split-ring compound planetary gearboxes for each joint has been done by using the following equations and constraints. A python program was made for us that parses through each and every possible gearbox configuration according to the constraints and gives the list of possible configurations for us to choose from for developing the gearbox.

$$R = S + (2 * P) \quad (1)$$

(For both input and output stages)

$$2 * \frac{S+P}{n} = whole\ number \quad (2)$$

(For both input and output stages)

$$D \leq \left(\frac{Pi}{2}\right) * Mi * sin\left(\frac{\pi}{n}\right) \quad (3)$$

$$Mo = \frac{Si+Pi}{So+Po} * Mi \quad (4)$$

$$Final\ Gear\ Ratio = \frac{1}{\frac{1}{Ro}\left(Ro - \frac{Ri*Pi}{Po}\right) * \frac{Si}{Ri+Si}} \quad (5)$$

The gearboxes were then designed according to the configurations selected. The selection of the configuration was done on the basis of the module of each stage of the gearbox and the number of planets in the gearbox. Factors such as the number of planet gears reduce the load exerted on individual teeth, but also introduce more surface area and hence increase friction. The pressure angle of the teeth of the gear was set to be 25 degrees to make the gears stronger, though again increasing the surface area and in return increasing the friction in the gearbox. The total area of teeth engagement for the planetary gearbox is also high and helps in the distribution of load across the surface of all the teeth engaged.

The output stage of the gearbox and the face of the planet gears and the output sun gear facing the output stage of the gearbox have been embossed with lines for making the alignment of gears while assembling easier. Along with lines, the planets are marked with numbers because the order of the planets' arrangement matters in such gearboxes. For axial rigidity of planet gears, there are cylindrical slots for 5mm chrome-plated steel rods in the planet gears. The insertion of these rods allows the gearbox to be more rigid and impervious to axial loads.

- Motor Assembly

The motor assembly consists of the components that are responsible for motor mounting and gearbox housing. The components are – the motor support, the motor, and the input ring cover for the gearbox. The motor support is just the component that provides support for the motor and mounts it to the body of the actuator. The motor support has slots for motor cooling and cable management. Along with support for the motor, this component plays the role of housing the bearing and is one of the mounting points of the *Theta*-Output Ring Cover Link.

The input ring cover component is the half of the gearbox housing that is holding the input stage of the gearbox. This component is also responsible for holding the motor so that the motor can be connected to the input stage of the gearbox. Inside the input ring cover, there is a slot for holding the hall sensor for the encoder setup. The components of the motor assembly are present for both *theta* and *fi* axis and are very similar. There are a few changes among the components of the two axis which are due to the mounting position of the respective components. The *fi*-motor support component is used to connect to the *theta*-output ring cover of another actuator joint and has a similar design to the *theta*-motor support component but the mounting design is different for both due to differences in where they are mounted or connected.

- *Theta*-Output Ring Cover Link (*Theta*-ORC Link)

  This is the component responsible for connecting the joint actuators with each other. This is connected to the output stage of the *theta-gearbox* and the *theta-motor* support component of an actuator. The next actuator is connected to the flat side of the *Theta*-Output Ring Cover Link through the *fi*-motor support component of the next actuator. This component is divided into two sections to make it easier to 3D Print. Also, this has a slot for a magnet that is used in conjunction with the hall sensor embedded in the *Fi* - Output Ring Cover for homing purposes.

- *Fi*-Output Ring Cover (*Fi*-ORC)

  This component holds together the components of the *theta* portion and the *fi* portion of the actuator. This is the middle link of the actuator joint which connects the output stage of the *fi* gearbox and the *theta* motor assembly. It has mounting holes for screwing in bolts that hold the assembly together. Also, this has a slot for a hall sensor, which is used here for homing purposes of the *theta-axis* of the actuator joint.

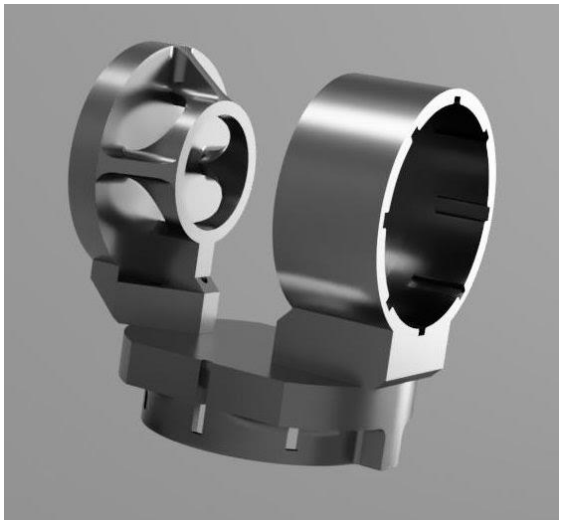

Fig 8. (left) *Theta*-Motor Support, (bottom) *Fi*-ORC, (right) *Theta*-IRC

3.2.2.2 The Gripper

The end effector of the robotic arm is a two-pronged parallel jaw gripper which is powered by a single MG995 servo motor. This end effector can be changed easily as the gripper is just mounted to the *theta*-output ring cover link of the wrist actuator joint.

The servo motor is used here to provide the required torque to hold onto the objects that this platform would be programmed to manipulate. The parallel jaw gripper was chosen as compared to other options because of its wide adoption in industrial robots. The gripper consists of three component assemblies - the jaw assembly, the servo rack, and the mounting plate. The mounting plate is a part upon which other component assemblies are mounted. This plate is then screwed onto the *theta*-output ring cover link. The servo rack is what houses the servo and is used to mount the servo onto the mounting assembly. The servo is connected to the jaw assembly via a link that is connected to one of the jaws and is intermeshed with a link that is connected to the other jaw.

The jaw assembly consists of two prongs of the gripper, a center block, and the links which connect the prongs to the center block. This block is mounted to the mounting plate and houses all the bearings that allow free rotation of the links connected to this. These links form a parallel linkage with the jaws which allows the jaws to always be parallel to each other. Each jaw is supported by three links, two of which contribute to the parallel linkage and the one left is the driver link which is either connected directly or is intermeshed with the servo motor.

The tips of the parallel jaws are customizable and changeable. The tips of the jaws for now are based on. They made a computational model, which predicted changes in the design of the gripper surface based on the success rate of the different designs throughout their design pool. Unlike the suggested material which is silicon-based resin, our gripper tips are made of TPU with a shore hardness of 90A. The infill percent of the model is changed to vary the flexibility of the tip according to the model suggested in the paper.

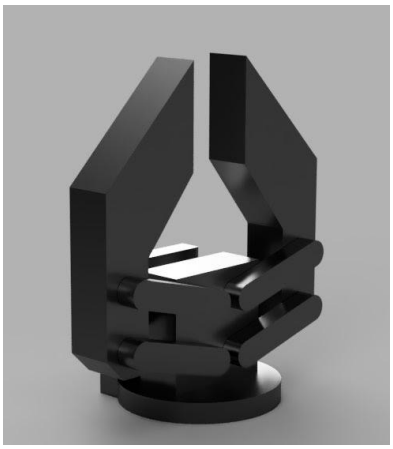

Fig 9. Render of our Parallel Jaw Gripper.

4. Benefits of our Design

The proposed platform is made using components that are readily available for cheap to researchers or start-ups for their research and development. The model components also support the targeted manufacturing method by being able to be printed without support material, which results in faster and more efficient printing of the components. The manufacturing method also allows rapid prototyping for the customizable add-ins or changes that the user might want to make to the model. The model is also open for any changes to the components used to make this platform; the motors are easily replaceable by making a few adjustments to the motor assembly components. The gearboxes are replaceable without any changes as long as their form factor is also cylindrical, which for most gearboxes is true.

The platform is scalable which broadens the scope of applications that this platform could be used for. The gearboxes can be made of any size required by using the program made and that could be the scaled-down or up version of the gearboxes used in the customized model.

5. Future Scope of Improvements

There is room for improvement in this design. Besides the hardware improvement that could deal with better motors and better encoders for accuracy, the end effector could be modified to be a variable end effector. This variable end effector could be programmed to change tools on the go with a mounted tool rack on the mobile base. The gearbox efficiency could be improved by using a self-lubricating material like nylon or other synthetic composites to have a smoother rotation. Further development of the platform will include an improved version of the gearbox, which we hope would increase the load-bearing capacity of each actuator. This study has an impact on practical implications and new views in the practice of robotic platforms. An in-depth analysis of factors affecting the efficiency of the planetary gearbox will be the basis of improvement in design further. Another improvement is to create a dedicated space for mounting a mapping or navigation like a stereoscopic camera setup or a LiDAR sensor. The variable end effector will also be part of the newer developed platform.

6. Conclusion

We have developed a platform that is capable of accomplishing general tasks of navigation and manipulation. The hardware that controls the platform is well capable of computing and running deep learning models for adaptive functionality and testing of some applications or tasks. The platform is easily manufactured and is considerably cheaper as compared to already available similar platforms. The proposed platform is a test bench that many small-scale researchers and startups can use to test and tune their software before deployment, and can also base their hardware on our platform.

Nomenclature

COP	coefficient of performance (–)
Si	Teeth count of the input sun gear
Ri	Teeth count of the input ring gear
Pi	Teeth count of the input planet gear
Mi	Gear Module of the Input Stage
N	Number of Planets
D	Inter Planet Clearance (mm)
So	Teeth count of the output sun gear
Ro	Teeth count of the output ring gear
Po	Teeth count of the output planet gear
Mo	Gear Module of the Output Stage

References

1) A. Ashwni, S. Gupta, and R. Rana, “Performance assessment of triangular obstacles mounted solar air heater using taguchi method,” *J. Eng. Res.*, (2021). doi:10.36909/jer.ICARI.15321.
2) A. Kaplish, A. Choubey, and R. Rana, “Design and kinematic modelling of slave manipulator for remote medical diagnosis,” *Int. J. Adv. Prod. Ind. Eng.*, **804** (*1*) 9–10 (2016).
3) A. Thakur, and R. Rana, “Traffic Noise Modelling Considering Traffic Compositions at Roundabouts,” in: 2021: pp. 657–672. doi:10.1007/978-981-15-8542-5_57.
4) G. Dutta, R. Kumar, R. Sindhwani, and R.K. Singh, “Digitalization priorities of quality control processes for smes: a conceptual study in perspective of industry 4.0 adoption,” *J. Intell. Manuf.*, **32** (*6*) 1679–1698 (2021). doi:10.1007/s10845-021-01783-2.
5) J. Nagpal, R. Rana, R. Lal, R. Muttanna Singari, and H. Kumar, “A brief review on various effects of surface texturing using lasers on the tool inserts,” *Mater. Today Proc.*, **56** 3803–3812 (2022). doi:10.1016/j.matpr.2022.01.272.
6) K. Raheja, A. Jain, C. Sharma, R. Rana, and R. Lal, “Comparative Study of Tribological Parameters of 3D Printed ABS and PLA Materials,” in: H. Adv. Manuf. Ind. Eng. Lect. Notes Mech. Eng. Springer, 2021: pp. 95–108. doi:10.1007/978-981-15-8542-5_9.
7) M.K. Chaudhary, A. Pathak, R. Goyal, R. Rana, and V.K. Sharma, “Fabrication of Aluminium 6082–B4C–Aloe Vera Metal Matrix Composite with Ultrasonic Machine Using Mechanical Stirrer,” in: 2021: pp. 221–229. doi:10.1007/978-981-15-8542-5_19.
8) R. Jindal, R. Arora, R. Papney, M. Patel, R. Chander Saini, and R. Rana, “Torsion test for a baja chassis using gyroscopic sensor and validation of cae results,” *Mater. Today Proc.*, **56** 3774–3779 (2022). doi:10.1016/j.matpr.2022.01.019.
9) R. Khanna, R. Maheshwari, A. Modi, S. Tyagi, A. Thakur, and R. Rana, “A review on recent research development on electric discharge machining (edm),” *Int. J. Adv. Res. Innov.*, **5** (*4*) 444–445 (2017).
10) R. Rana, L. Krishnia, Q. Murtaza, and R.S. Walia, “Optimizing the machining performance of cnc tools inserts coated with diamond like carbon coatings under the dry cutting environment,” *J. Eng. Res.*, (2021). doi:10.36909/jer.ICARI.15327.
11) R. Rana, L. Krishnia, R.S. Walia, and Q. Murtaza, “CVD diamond coated tungsten carbide (wc) tool inserts,” *J. Eng. Res.*, (2021). doi:10.36909/jer. ICARI.15319.
12) R. Rana, Q. Murtaza, and R.S. Walia, “GA based optimization of tri-bological behaviour of diamond coated tungsten carbide,” *World J. Eng.*, **17** (*3*) 335–

346 (2020). doi:10.1108/WJE-08-2019-0220.
13) R. Rana, Q. Murtaza, and R.S. Walia, "Optimization using genetic algorithm of tribological behaviour of wc tool material," *Indian J. Eng. Mater. Sci.*, **27** (*4*) 889–896 (2020).
14) R. Rana, R.S. Walia, and Q. Murtaza, "Characterization and parametric optimization of performance parameters of dlc-coated tungsten carbide (wc) tool using topsis," *Coatings*, **11** (*7*) 760 (2021). doi:10.3390/coatings11070760.
15) R. Rana, W. R.S., and Q. Murtaza, "Characterizing and analyzing the tribological behaviour of diamond coated tungsten carbide (wc)," *J. Eng. Res.*, (2022). doi:10.36909/jer.ICAPIE.15107.
16) R. Singh, D. Sachan, R. Verma, S. Goel, R. Jayaganthan, and A. Kumar, "Mechanical behavior of 304 austenitic stainless steel processed by cryogenic rolling," *Mater. Today Proc.*, **5** (*9*) 16880–16886 (2018). doi:10.1016/j.matpr.2018.04.090.
17) S. Bansal, A. Saraf, R. Rana, and R. Lal, "Effect of Picosecond Laser Texture Surface on Tribological Properties on High-Chromium Steel Under Non-lubricated Conditions," in: 2021: pp. 257–267. doi:10.1007/978-981-15-8542-5_22.
18) S.K. Tiwari, and S.K. Garg, "Comparison of coronary heart disease prediction models using various machine learning algorithms," *J. Eng. Res.*, (2021). doi:10.36909/jer.ICARI.15323.
19) V.K. Sharma, S.K. Rana, R. Lal, and R. Rana, "Wear and residual stress analysis of waste sea shell and b4c particles reinforced green hybrid aluminium metal composite," *J. Eng. Res.*, (2021). doi:10.36909/jer.ICARI.15317.
20) A. Gupta, S. Lata, R. Rana, and R. Lal, "A Statistical Approach for Overcut and Burr Minimization During Drilling of Stir-Casted MgO Reinforced Aluminium Composite," in: 2021: pp. 269–283. doi:10.1007/978-981-15-8542-5_23.
21) D. Singh, S. Lata, and R. Rana, "Reverse engineered structure of tool post aiding tool tip alignment with work center," *Mater. Today Proc.*, **5** (*2*) 6433–6443 (2018). doi:10.1016/j.matpr.2017.12.256.
22) Sanjeev Kumar Lambha, V. Kumar, and R. Verma, "Impact of liner elasticity on couple stress lubricated partial bearing," *Evergreen*, **9** (*1*) 56–71 (2022). doi:10.5109/4774217.
23) J.A. Hidayat, and B. Sugiarto, "Characteristic, structure, and morphology of carbon deposit from biodiesel blend," *Evergreen*, **7** (*4*) 609–614 (2020). doi:10.5109/4150514.
24) Nor Athira Jamaluddin, N. Talib, and Amiril Sahab Abdul Sani, "Performance comparative of modified jatropha based nanofluids in orthogonal cutting process," *Evergreen*, **8** (*2*) 461–468 (2021). doi:10.5109/4480729.
25) A. Y, S. S, H. H, and M.. Musa, "Friction characteristic study on flat surface embedded with micro pit," *Evergreen*, **8** (*2*) 304–309 (2021). doi:10.5109/4480707.
26) N. Talib, Nor Athira Jamaluddin, Tan Kai Sheng, Lee Woon Kiow, H. Abdullah, S. Ahmad, and A. Saleh, "Tribological study of activated carbon nanoparticle in nonedible nanofluid for machining application," *Evergreen*, **8** (*2*) 454–460 (2021). doi:10.5109/4480728.
27) V. Gupta, and A. Jayant, "A novel hybrid mcdm approach followed by fuzzy dematel-anp-topsis to evaluate low carbon suppliers," *Evergreen*, **8** (*3*) 544–555 (2021). doi:10.5109/4491640.
28) N. Nisrina, Muhammad Irfan Kemal, Ilham Ali Akbar, and T. Widianti, "The effect of genetic algorithm parameters tuning for route optimization in travelling salesman problem through general full factorial design analysis," *Evergreen*, **9** (*1*) 163–203 (2022). doi:10.5109/4774233.